REPORT DOCUMENTATION PAGE

Form Approved OMB NO. 0704-0188

1. REPORT DATE (DD-MM-YYYY)	2. REPORT TYPE	3. DATES COVERED (From - To)
	New Reprint	-

4. TITLE AND SUBTITLE
Enhanced Fuel Cell Catalyst Durability with Nitrogen Modified Carbon Supports

5a. CONTRACT NUMBER
W911NF-09-1-0528

5b. GRANT NUMBER

5c. PROGRAM ELEMENT NUMBER
611103

6. AUTHORS
T. S. Olson, A. A. Dameron, K. Wood, S. Pylpenko, K. E. Hurst, S. Christensen, J. B. Bult, D. S. Ginley, R. O'Hayre, H. Dinh, T. Gennett

5d. PROJECT NUMBER

5e. TASK NUMBER

5f. WORK UNIT NUMBER

7. PERFORMING ORGANIZATION NAMES AND ADDRESSES
Colorado School of Mines
Research Administration
1500 Illinois St
Golden, CO 80401 -1911

8. PERFORMING ORGANIZATION REPORT NUMBER

9. SPONSORING/MONITORING AGENCY NAME(S) AND ADDRESS(ES)
U.S. Army Research Office
P.O. Box 12211
Research Triangle Park, NC 27709-2211

10. SPONSOR/MONITOR'S ACRONYM(S)
ARO

11. SPONSOR/MONITOR'S REPORT NUMBER(S)
54646-CH-PCS.21

12. DISTRIBUTION AVAILIBILITY STATEMENT
Approved for public release; distribution is unlimited.

13. SUPPLEMENTARY NOTES
The views, opinions and/or findings contained in this report are those of the author(s) and should not contrued as an official Department of the Army position, policy or decision, unless so designated by other documentation.

14. ABSTRACT
Thiswork illustrates the utility and improved performance of nitrogen-modified catalyst supports for direct methanol fuel cell (DMFC)
applications. A unique two-step vapor-phase synthesis procedure is used to achieve the N-modification and Pt-Ru decoration of high
surface-area carbon powders relevant to integration as electrocatalysts in fuel cell membrane electrode assemblies

15. SUBJECT TERMS
fuel cell, methanol, catalysis, durability, nitrogen modification

16. SECURITY CLASSIFICATION OF:			17. LIMITATION OF ABSTRACT	15. NUMBER OF PAGES	19a. NAME OF RESPONSIBLE PERSON
a. REPORT	b. ABSTRACT	c. THIS PAGE			Ryan O'Hayre
UU	UU	UU	UU		19b. TELEPHONE NUMBER 303-273-3952

Report Title

Enhanced Fuel Cell Catalyst Durability with Nitrogen Modified Carbon Supports

ABSTRACT

Thiswork illustrates the utility and improved performance of nitrogen-modified catalyst supports for direct methanol fuel cell (DMFC)
applications. A unique two-step vapor-phase synthesis procedure is used to achieve the N-modification and Pt-Ru decoration of high
surface-area carbon powders relevant to integration as electrocatalysts in fuel cell membrane electrode assemblies (MEA's). First,
nitrogen surface moieties are incorporated into a commercial high surface area carbon support via a N-ion implantation technique,
followed by Pt-Ru nanoparticle deposition via magnetron sputtering. The nitrogen-ion implantation of high surface area carbon
supports yields superior Pt-Ru catalyst particle stability and performance as compared to industry standards. Specifically, results
indicate a higher retention of metal catalyst surface area and electrochemical activity after accelerated electrochemical degradation
testing. Further, characterization of catalyst materials before, during and after the electrochemical cycling provides insight into the
catalyst particle coarsening and/or catalyst surface area loss mechanisms that dominate this fuel cell catalyst system.

REPORT DOCUMENTATION PAGE (SF298)
(Continuation Sheet)

Continuation for Block 13

ARO Report Number 54646.21-CH-PCS
Enhanced Fuel Cell Catalyst Durability with Nitro ...

Block 13: Supplementary Note

Approved for public release; distribution is unlimited.

Journal of The Electrochemical Society, **160** (4) F389-F394 (2013)
0013-4651/2013/160(4)/F389/6/$31.00 © The Electrochemical Society

Enhanced Fuel Cell Catalyst Durability with Nitrogen Modified Carbon Supports

Tim S. Olson,[a] Arrelaine A. Dameron,[a] Kevin Wood,[b,*] Svitlana Pylpenko,[b] Katherine E. Hurst,[a,] Steven Christensen,[a] Justin B. Bult,[a] David S. Ginley,[a,***] Ryan O'Hayre,[b] Huyen Dinh,[a] and Thomas Gennett[a,z]**

[a]*National Renewable Energy Laboratory, Golden, Colorado 80401, USA*
[b]*Colorado School of Mines, Metallurgical and Materials Engineering, Golden, Colorado 80401, USA*

This work illustrates the utility and improved performance of nitrogen-modified catalyst supports for direct methanol fuel cell (DMFC) applications. A unique two-step vapor-phase synthesis procedure is used to achieve the N-modification and Pt-Ru decoration of high surface-area carbon powders relevant to integration as electrocatalysts in fuel cell membrane electrode assemblies (MEA's). First, nitrogen surface moieties are incorporated into a commercial high surface area carbon support via a N-ion implantation technique, followed by Pt-Ru nanoparticle deposition via magnetron sputtering. The nitrogen-ion implantation of high surface area carbon supports yields superior Pt-Ru catalyst particle stability and performance as compared to industry standards. Specifically, results indicate a higher retention of metal catalyst surface area and electrochemical activity after accelerated electrochemical degradation testing. Further, characterization of catalyst materials before, during and after the electrochemical cycling provides insight into the catalyst particle coarsening and/or catalyst surface area loss mechanisms that dominate this fuel cell catalyst system.
 [DOI: 10.1149/2.062304jes]

Manuscript submitted October 19, 2012; revised manuscript received January 30, 2013. Published February 12, 2013.

State-of-the-art low-temperature direct methanol fuel cell (DMFC) electroxidation catalysts typically consist of a Pt-Ru alloy particle phase supported on carbon black. Enhancements in the methanol oxidation activity and/or the Pt-Ru particle stability can provide increased energy conversion efficiencies in DMFC systems and push the technology toward mainstream commercialization. In this study, high surface area catalyst materials for DMFC anode applications are functionalized with nitrogen and are characterized in order to elucidate the mechanism for improved catalyst particle stability that results from N-modification. This effort builds on our recent planar system model studies that highlighted the potential of nitrogen-functionalization to increase carbon-supported Pt and PtRu electrocatalysts by beneficially tuning catalyst-support interactions.[1–4]

In DMFCs, CO-related intermediate-species poisoning during methanol electrooxidation can be ameliorated by employing bimetallic (most commonly PtRu) alloy catalysts in preference to pure Pt catalysts.[5,6] Unfortunately, one side effect of utilizing Pt-Ru based anode catalyst materials is Ru-crossover, which leads to performance losses.[7–9] Further, loss of active catalyst surface area due to particle growth mechanisms such as migration/coalescence and Oswald ripening also contribute to the overall performance degradation. Developing material-based solutions to mitigate the effect of Ru-crossover as well as limiting particle growth processes are highly desired. Here we demonstrate that the enhanced catalyst particle stability provided by tuning catalyst-support interactions through nitrogen modification of high surface area carbon supports can mitigate these Ru crossover and particle-growth degradation mechanisms.

Previously, we reported on the effects of nitrogen modification in a planar model system using highly oriented pyrolitic graphite (HOPG), with potential catalyst synthesis routes to alleviate the effect of Ru-crossover while also increasing catalyst particle stability to minimize the loss of catalyst surface area due to agglomeration.[1,3,4,10] Our approach involved modification of the surface of highly oriented pyrolitic graphite (HOPG) substrates with nitrogen using an ion-implantation technique with subsequent deposition of the nanoparticle catalyst phase. With this model system, we were able to establish the catalyst degradation mitigation processes and support chemistries beneficial to fuel cell systems. We found that Pt-Ru nanoparticles deposited on N-modified HOPG substrates were more stable under electrochemical potential cycling as compared to unmodified or argon implanted HOPG substrates. We postulated that incorporation of nitrogen into the surface layers of the carbon support created heteroatomic carbon-nitrogen regions which enhanced catalyst nanoparticle-support interactions and increased nanoparticle stability.[1,4,10] Specifically, pyridinic-type nitrogen surface defects have been speculated to play a role in the improved stability of noble metal nanoparticles catalyst.[11–13] Another advantage of N-containing catalyst supports reported in the literature is improved MOR reaction onset potentials.[1,14–23] This observation is particular prevalent when compared to internal benchmarks.

This work focuses on the N-functionalization of high surface-area carbon powders relevant to integration in fuel cell membrane electrode assemblies (MEA's) through a two-step synthesis procedure. First, nitrogen heteroatoms are incorporated into a commercial high surface area carbon support via a N-ion implantation technique, followed by Pt-Ru incorporation via magnetron sputtering. Both ion-implantation and sputtering processes are performed in a single chamber without breaking vacuum. Through electrochemical testing, microscopy, X-ray photoelectron spectroscopy (XPS), small-angle X-ray scattering (SAXS), and X-ray diffraction (XRD), this work illustrates the unique electrochemical performance of the new materials. Overall, the nitrogen-functionalized high surface-area catalyst materials demonstrate similar enhancements in stability as we previously described for the model HOPG,[1,3] and outperform benchmark commercial catalyst in terms of both activity and stability.

Experimental

Catalyst synthesis (ion-implantation and physical vapor deposition).— Powder catalyst samples were fabricated in a custom sputter chamber described in detail elsewhere.[24] The chamber, consisting of vacuum components and backed by a 520 L/s turbo molecular pump (Balzers TMP 520, Pfeiffer Vacuum GmbH, Asslar, Germany), housed a rotating barrel type powder sample holder rotated with a DC gear motor (Leeson Electric Corporation, Grafton, WI), an ion source (3 cm DC (ITI) ion gun, Veeco, Santa Barbara CA) and an orthogonally-oriented 2" sputter gun (Onyx Mag 2, Angstrom Sciences, Duquesne, PA). The ion gun was positioned a distance of 9 inches at 35 degrees from normal to the powder surface. The retractable sputter gun was at a sample-to-target distance of 2.6". (Figure 1). During implantation and deposition, the barrel was rotated at 30 rpm, in order to achieve uniform modification of the samples. During ion-implantation, the sputter gun was retracted to be clear of the incident ion beam (Figure 1A). For sputtering, the

*Electrochemical Society Student Member.
**Electrochemical Society Active Member.
***Electrochemical Society Fellow.
zE-mail: Thomas.Gennett@nrel.gov

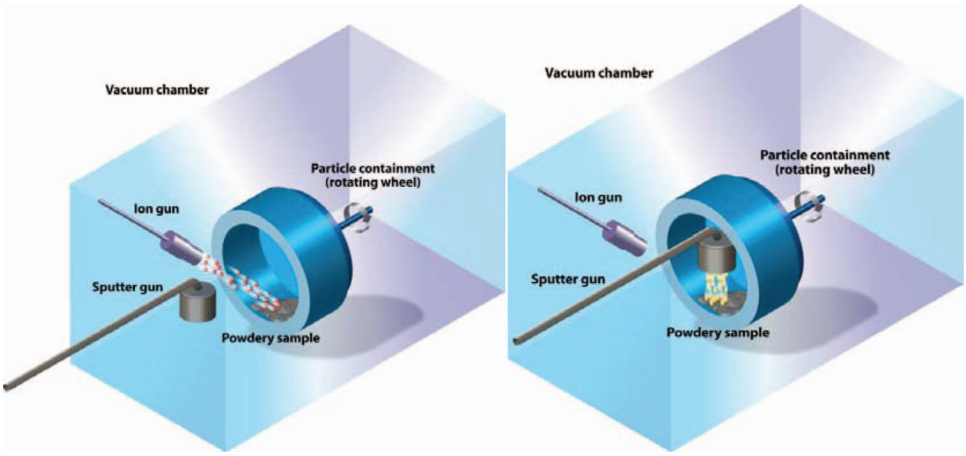

Figure 1. Schematic of the vacuum chamber used for catalyst synthesis. Ion-implantation and Pt-Ru sputter deposition are carried out step-wise in the fabrication chamber.

sputter gun head is positioned inside the wheel to allow for free rotation. (Figure 1B). Sputter process gases were introduced through a MFC controlled manifold while implantation gases were introduced directly via a separate leak valve directly through the ion gun. During an experiment, 500–1000 mg of commercially available carbon powder (Cabot Vulcan XCR72R) was placed into the barrel and the chamber was evacuated to approximately 1×10^{-6} Torr. Implantation was performed prior to sputtering at a chamber pressure of 1×10^{-4} Torr N_2. The beam current and implantation times were held constant for a particular sample in the range of 12 mA to 45 mA, and 15 mins to 120 mins, respectively. Discharge and acceleration voltage were held constant at 55 V and 100 V, respectively, for all samples. Following implantation, sputter depositions were performed at 25 mTorr with 10 mol% O_2:Ar at DC power of 45 W for 60 mins. The chamber was not opened in-between implantation and sputtering, which limited any oxidation of the modified support surface. Optimization of the Pt-Ru sputter parameters for these high surface area catalyst supports has been reported elsewhere.[24]

The composite inks of the electrode materials for half-cell electrochemical testing consisted of 10 mg of catalyst powder, 7.96 mL of 18 MΩ DI water, 2 mL of isopropyl alcohol and 40 μL of 5 wt% Nafion solution (total catalyst concentration of 1 mg/mL). The ink was bath-sonicated in ice water for 20 minutes to generate a stable homogeneous catalyst ink solution. A 10 μL aliquot of the dispersed ink solution was placed on a 0.196 cm^2 glassy carbon electrode and dried in air. The electrochemical 3-electrode half-cell was completed with a Pt-mesh counter electrode and a calomel reference electrode (235 mV vs. RHE) separated from the main cell via a salt bridge.

Carbon monoxide (CO) stripping experiments were performed in 0.5 M H_2SO_4 by saturating the electrolyte with CO and holding the working electrode at a potential of 0.2 V vs. RHE for 10 minutes at 25 C (room temp). The cell was then purged with N_2 for 15 minutes while the electrode potential was maintained at 0.2 V vs. RHE. The potential was then scanned in the positive direction to 0.9 V at 20 mV/s. The upper potential limit of 0.9 V was implemented for Accelerated Degradation Testing (ADT). This ADT protocol allows us to obtain data in a short amount of time and correlate DMFC catalyst stability and degradation with the results of the ADT.Two subsequent full potential sweeps (0 to 0.9 V vs. RHE) were collected and used as the background for determination of CO stripping area. Methanol oxidation testing was performed in N_2 saturated 0.5 M H_2SO_4/0.5 M methanol solution (room temp). The potential was swept from 235 mV to 800 mV vs. RHE at 10 mV/s.

The catalyst-substrate metal composition was determined by X-ray fluorescence (XRF) with a maXXi 5/PIN XRF instrument (Roentgen Analytic) equipped with a tungsten target. The XRF composition was calibrated to a series of $Pt_{1-x}Ru_x$ standards. The transmission Electron Microscopy (TEM) micrographs of Pt-Ru nanoparticles supported on unmodified and N-modified Vulcan were obtained on a Philips CM200 TEM. X-ray Photoelectron Spectroscopy (XPS) analysis of the synthesized catalysts was done on a Kratos Nova XPS with a monochromatic Al K-alpha source operated at 300 W. Survey and high-resolution spectra were acquired from a minimum of three areas per sample. Data analysis was performed using CasaXPS software and included subtraction of the linear background for O 1s and N 1s. The Shirley background for Pt 4f, Ru 3p and combined C 1s/Ru 3d regions and charge referencing using the graphitic peak at 284.6 eV.

The electrodes for the in-situ Small Angle X-ray Spectroscopy (SAXS) and X-ray diffraction (XRD) experiments were prepared by applying catalyst ink drop-wise to SGL Group company Carbon 25BA gas diffusion backing paper. The inks were prepared to produce electrode catalyst layers with 1:1 carbon:Nafion ratios and total metal loadings of approximately 5 mg.

XRD was performed on the 11-3 beam line at the Stanford Synchrotron Radiation Light source (SSRL) at SLAC National Accelerator Laboratory. The beam line employs a side-deflecting, bent Si (311) monochromator to select X-rays at 12.724 keV off an insertion device. No calibration of the flux was performed. The data were collected on an image plate (MAR345) and reduced using the WxDiff software platform. Data are plotted as intensity versus magnitude of the momentum transfer vector, $q = 4\pi/\lambda\sin\theta$ where λ is the X-ray wavelength and θ the angle between the incident X-rays and sample surface. The q calibration was performed during data reduction using the diffraction rings from lanthanum hexaboride powder.

SAXS was conducted on beam line 1–4 of SSRL at SLAC National Accelerator Laboratory. Data was collected at incident photon energy of 8.33 keV using a Rayonix 165 CCD detector. The collected data was then analyzed with the Igor Pro (v. 6.22, Wavemetrics) plug-in, Irena (v. 2.40). Samples subjected to approximately 3000 electrochemical cycles, while the X-ray spot remained in the same location. For each spectrum acquired, background was subtracted to zero and the contribution from the carbon backing was removed. The intensities were subsequently fitted as a function of probability using two lognormal distributions. This process was performed for all three catalysts.

The X-ray experiments were conducted using a custom-built cell specifically designed for in-situ *measurements*. The cell operates in transmission mode with a working electrode constructed of carbon paper modified with catalyst material suspended in solution. The window materials consisted of 6 μm Kapton (Chemplex Industries, Inc). The transmission path for an empty cell included ∼12 μm of Kapton and ∼0.5 mm of electrolyte solution. The cell also had a small reservoir (∼50 mL) for solution and spaces to hold a platinum mesh counter electrode. Another compartment in the cell allowed for connection to the $Ag+/AgCl_2$ reference electrode (BASi, Part No. MF2052) via a

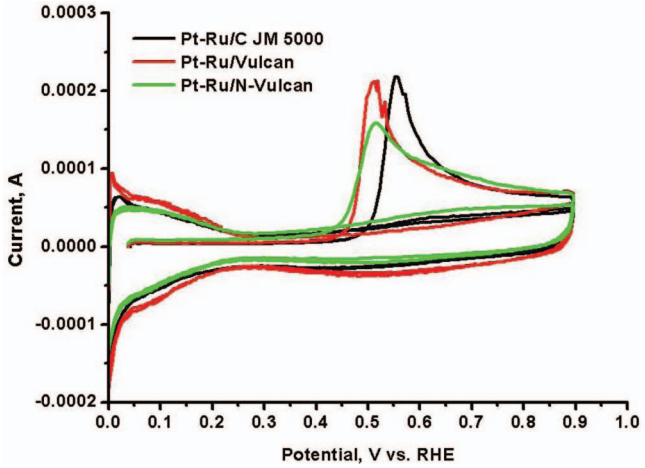

Figure 2. CO stripping curves obtained for the undoped, doped, and commercial Pt-Ru materials.

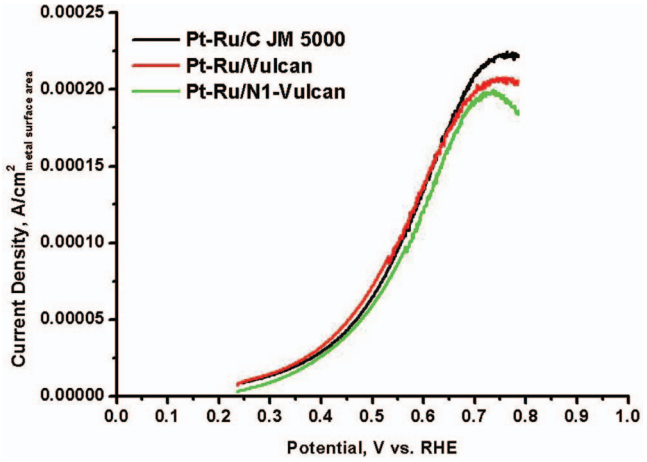

Figure 3. MeOH oxidation currents normalized to CO stripping surface area for the undoped, doped, and commercial Pt-Ru materials.

salt bridge. We used a 0.1 M perchloric acid solution (GSF Chemicals). Typical waveforms consisted of cyclic sweeps from 0 to 0.9 V vs. RHE with a 0.5 V/s scan rate.

Results and Discussion

In this work the characterization and electrochemical performance of three sets of Pt-Ru based fuel cell catalyst materials supported on carbon or N-modified carbon were investigated. The materials included: commercially available Johnson Matthey Pt-Ru/C catalyst (JM 5000); an in-house material utilizing a non-modified carbon support (Pt-Ru/C); and an in-house material fabricated with N-modified carbon support (Pt-Ru/N-C).

XPS surface characterization of heteroatom modified fuel cell catalyst support materials.— XPS analysis of the three catalyst materials showed that the elemental concentration of nitrogen ranged from 0.2 at% for the undoped in-house support, to 0.5 at% for the JM 5000 commercial benchmark, to 1.3 at% for the in-house N-doped sample implanted at 14 mA. The increase in the N concentration for the N-doped sample was also accompanied by the broadening of the C 1s spectra (not shown) caused by the formation of various C-N as well as C-O bonds.[10] The small amounts of nitrogen detected in the undoped and JM5000 materials are related to the presence of a single nitrogen peak attributed to either amine, cyano or pyrrolic nitrogen. In general, we have observed that the N 1s spectra for implanted samples are much broader, indicative of the presence of various nitrogen functionalities, including pyrrolic, pyridinic, amine and graphitic N.

The *bulk* Ru:Pt ratio, measured with X-ray fluorescence (XRF), consistently indicates that sputtered materials are slightly enriched in platinum as compared to the commercial catalyst benchmark. However, the *surface* Ru:Pt ratio, as measured by XPS, indicates enrichment in ruthenium with the N-modified samples as compared to the non-implanted commercial and in-house sputtered samples. Overall we found a major difference between commercial and sputtered samples with respect to their ruthenium compositions with the results summarized in Table I. In commercial catalysts, surface ruthenium is distributed between metallic ruthenium (Ru(0), Ru(II), Ru(IV), ruthenium oxide RuO_2 and hydrous ruthenium oxide $RuO_2 \cdot nH_2O$,[4,25] whereas the in-house catalysts show significantly greater amounts of hydrous ruthenium oxide $RuO_2 \cdot nH_2O$ but significantly lower amounts of Ru(0), Ru(II), and RuO_2.

Fuel Cell catalyst electrochemical performance.— Determination of the electrochemical surface area (ECSA) for the various Pt-Ru/C and Pt-Ru/N-C materials was accomplished with standard CO stripping analysis (420 $\mu C/cm^2$). Figure 2 shows the CO stripping curves for the in-house fabricated materials as well as commercially available 30 wt% Pt-Ru/C (JM 5000). All in-house materials show a more negative "*kick-off*" potential for the removal and oxidation of the adsorbed CO as compared to the commercial benchmark. The N-modified carbon supported catalysts indicate lower ECSA (55 m^2/g) as compared to the non-modified carbon supported catalysts (69–73 m^2/g). Based on this data and the overall Pt-Ru metal contents of the respective catalyst materials, the mass-specific surface areas ($m^2_{Pt\text{-}Ru}/g_{Pt\text{-}Ru}$) were calculated and the values are shown in Table II. The methanol oxidation curves normalized to the CO stripping surface area shown in Figure 3 which illustrates that the specific and mass activity at 0.4 V for the in-house materials is almost identical to that of the commercial benchmark (values are listed in Table II).

Accelerated electrochemical degradation tests (ADT) were performed by cycling the electrode potential from 0 to 0.9 V vs. RHE. The CO stripping areas were measured after 0, 100, and 5000 electrochemical potential cycles. Since a DMFC anode is rarely brought to poten-

Table I. Quantification of Pt-Ru/Carbon materials demonstrating elemental composition, determined by XPS, distribution of ruthenium species obtained by curve-fitting Ru 3p spectra and ratio of ruthenium to platinum, determined by XPS and XRF.

	Elemental concentration, XPS Relative concentration, at%					Ru:Pt ratio		Distribution of ruthenium, XPS, relative concentration,%			
Sample	C	O	Pt	Ru	N	XPS	XRF	Ru_1, Ru	Ru_2, RuO_2 screened final state	Ru_3, $RuO_2 \cdot nH_2O$	Ru_4, RuO_2 unscreened final state
Pt-Ru/C JM5000,	89.3	7.8	1.2	1.3	0.5	1.1	0.99	10.7	32.1	38.7	18.6
sputtered, undoped	85.9	9.9	1.9	2.0	0.2	1.1	0.91	0.0	10.1	50.6	39.3
sputtered, doped, 14 mA	88.3	7.4	1.4	1.6	1.3	1.2	0.93	0.0	6.8	52.9	40.3

Table II. The values for Electrochemical Area (ECA) as determined by CO stripping, the MOR specific activities, and percentage of ECA after 100× and 5000× cycles in the ADT protocol are tabulated.

Catalyst	ECA (m^2/g)	Specific Activity @ 0.4 V (A/cm^2_{metal})	Mass Activity @ 0.4 V (A/mg_{metal}) × 10^3	% of ECA after 100 × durability cycles	% of ECA after 5000 × durability cycles
Pt-Ru/Vulcan	73	3.3×10^{-5}	24	51	10
Pt-Ru/N-Vulcan	55	2.9×10^{-5}	17	60	40
Pt-Ru/C JM 5000	69	3.0×10^{-5}	20	48	17

tials higher than 0.7 V during typical fuel cell operation and because an increased rate of Ru dissolution at potentials greater than 0.9 V is common, this limited potential cycling window was chosen for accelerated durability testing.[26] Figure 4 shows the stripping curves for the materials while the calculated percent of remaining ECSA after 100× and 5000× cycles are shown in Table II. Compared to the unmodified catalysts, the N-modified Pt-Ru/N-Vulcan catalyst shows a higher retention of metal surface area after the ADT. We postulate that in the sputter deposition the metal phase does not preferentially nucleate and grow in the most energetically favorable locations. This explains the similar initial electrochemical behavior of the unmodified vs. N-modified catalysts. However, upon electrochemical cycling, improved durability is obtained for PtRu nanoparticles fortunate enough to be associated with nitrogen defect clusters in the N-modified catalyst.

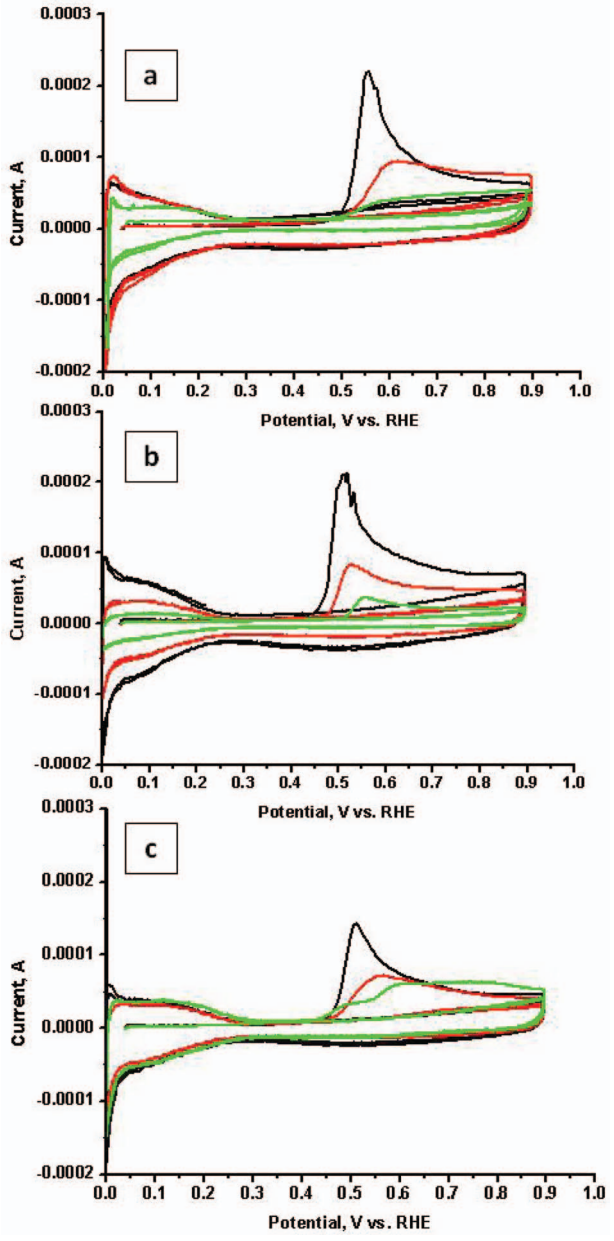

Figure 4. CO stripping curves obtained after 0 (black), 100 x (red), and 5000 x (green) cycles for (a) Pt-Ru/C JM5000, (b) Pt-Ru/Vulcan (undoped), and (c) Pt-Ru/N-Vulcan (N-doped).

Evidence for improved catalyst particle stability on N-modified supports.— Detailed characterization of the fuel cell catalyst materials before and after the ADT allowed us to evaluate the degradation processes that contributed to catalyst surface area loss and diminished energy conversion efficiency. Figure 5 shows TEM micrographs that were obtained before (a, c, e) and after the cycling (b, d, f) protocol for each material. Inspection of the micrographs indicates that the unmodified catalyst materials (both commercial (a and b) and in-house (c and d)) show a loss in particle density as well as particle coarsening/agglomeration. In contrast, the N-modified material (d and f) maintained the pre-cycled particle density and size distribution. Although some limited particle growth is observed for the N-modified catalyst system, significantly less surface area loss is recorded. These observations directly support the electrochemical surface area observations (from the CO stripping experiments) that the N-modified catalyst material maintained higher percentage of the initial metal surface areas.

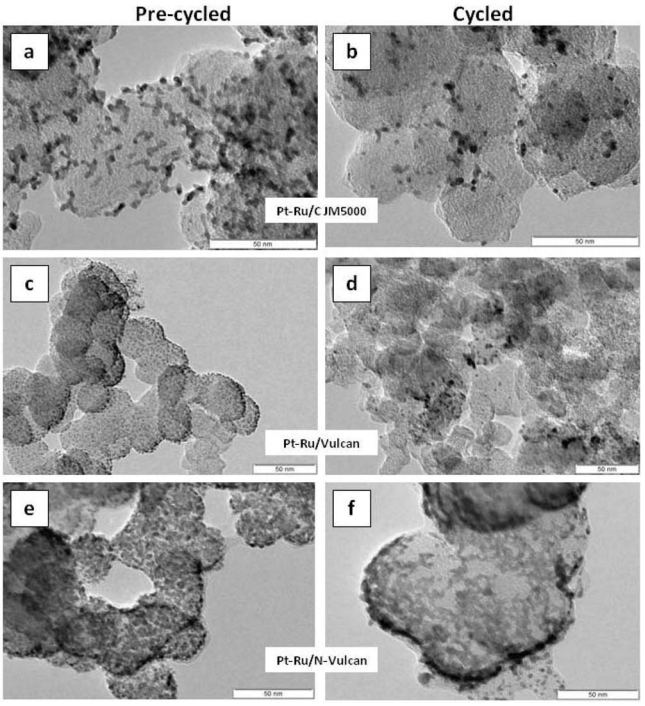

Figure 5. TEM micrographs obtained for pre-cycled (a, c, e) and cycled (b, d, f) supported Pt-Ru materials.

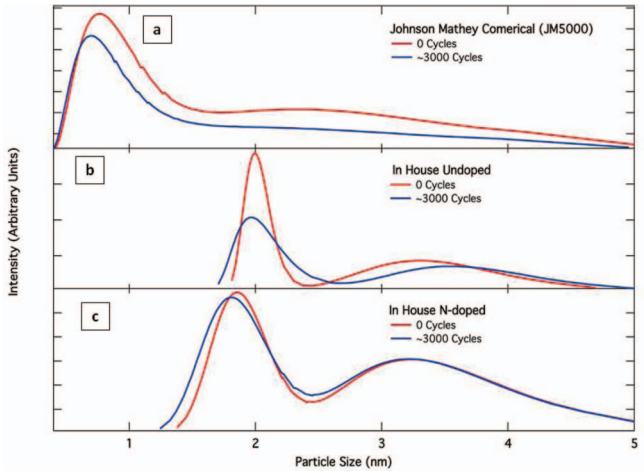

Figure 6. in-situ SAXS spectra after 0 (blue) and 3000 (red) electrochemical potential cycles for (a) Pt-Ru/C JM5000, (b) Pt-Ru/Vulcan (undoped), and (c) Pt-Ru/N-Vulcan (N-doped).

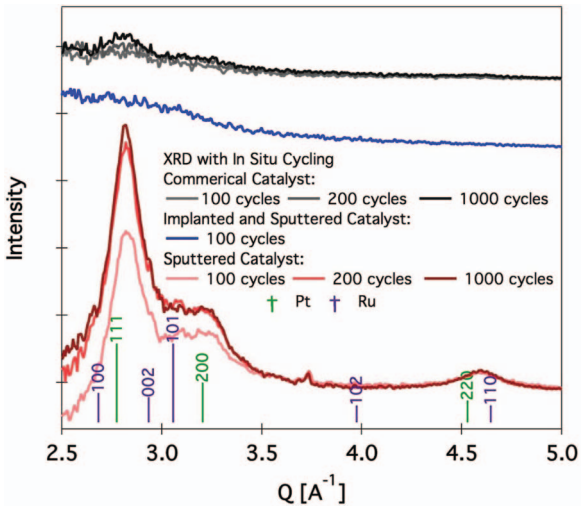

Figure 7. XRD difference spectra for the commercial catalyst (Pt-Ru/C JM5000), implanted and sputtered (Pt-Ru/N-Vulcan), and the sputtered (Pt-Ru/Vulcan) materials obtained during in-situ potential cycling. Each spectrum is the mathematical difference between the cycling spectrum and the initial un-cycled spectrum.

In-situ SAXS experiments were performed to further assesses the changes that occur to the catalysts during potential cycling. This in-situ technique enabled specific, identical regions of the electrodes to be compared before and after potential cycling in order to eliminate the variability issues associated with the heterogeneous nature of the materials at different regions of the electrodes. With SAXS, both the crystalline and amorphous phases of the Pt-Ru catalyst nanoparticles are analyzed. Figure 6 shows the scattering diameter-volume distributions for the Pt-Ru particle phases before and after 3000 electrochemical potential cycles (0 V to 0.9 V vs. RHE). The commercial catalyst (Figure 6a) shows a decrease in the volume distribution across the entire 1–5 nm particle range, which is most likely due to dissolution. (Although information is not provided by the manufacturer, the JM500 catalyst is widely believed to be fabricated using the industrial standard colloidal deposition technique to achieve the small particle size.) In significant contrast, the N-modified catalyst exhibits almost no change in volume distribution after cycling (Figure 6c). The most prevalent change is observed on the unmodified in-house sputtered catalyst material (Figure 6b). Here, the cycling protocol resulted in significant losses of the ∼2 nm particle size distribution and a shift in the larger particle distribution peak from 3.25 nm to 3.75 nm. Based on this data alone it is difficult to distinguish between which particle growth processes are responsible for the observed changes in particle-size distribution. However, further speculation on the particle growth process in this system is enabled by coupling this data with XRD analysis.

As XRD only yields information on crystalline phases, a comparison of the SAXS vs. XRD data provides insight to distinguish between agglomeration vs. dissolution/re-deposition particle growth processes. If the re-deposition of the dissolved metal phase is the primary particle growth mechanism, then growth of crystalline peaks in the XRD spectrum is expected. Figure 7 shows the changes in the diffraction patterns induced by cycling the in-house doped and undoped materials as well as the JM 5000 commercial standard. Each "difference spectra" in Fig. 7 represents the mathematical difference between a spectrum acquired after a certain number of electrochemical cycles vs. the initial uncycled material spectrum. These difference spectra can be computed because exactly the same area of the sample is examined before and after cycling in the synchrotron using the in-situ electrochemical cell setup. A series of difference spectra, taken after increasing numbers of electrochemical cycles, are shown for each catalyst. For all samples, the initial spectra (at 0 cycles, not shown) lacked any peak structure This lack of peak structure indicates that catalyst materials lack long-range order i.e., the metal catalyst phases are non-crystalline and more amorphous. As a function of cycling, the undoped in-house catalyst (red spectra) developed several crystalline peaks indicative of a Pt-Ru alloy material. The crystalline peaks grew quickly, within the first 150 cycles, and then remained unchanged for the duration of the cycling experiments. This data suggests a growth and stabilization mechanism with dissolution of particles balanced by growth through re-deposition, migration and coalescence processes. In contrast, the commercial catalyst (black spectra) changed minimally, and discernible crystalline peaks were only apparent after ∼1000 cycles. The emergence of these peaks, the dominant Pt-Ru alloy peaks, shifted to slightly higher Q from Pt ⟨111⟩ and Pt ⟨002⟩, suggest a similar degradation mechanism, although the catalyst is stabilized significantly compared to the in-house undoped catalyst. The doped in-house catalyst (blue spectra), at initial cycling times, appears much more stable than the undoped in-house catalyst. At 100 cycles, no appreciable peak signature can be discerned from the noise. These data demonstrate that N-doping within the catalyst-carbon matrix blocks or delays the degradation of the sputtered catalyst materials by increasing the catalyst support interactions. We are able to correlate the emergence of the XRD peak in in-house undoped catalyst upon ADT cycling with the growth of the ∼12 nm particle size regime in Figure 5d. Further, the loss of ECSA as determined by CO stripping also supports these observations.

Catalyst surface area loss mechanisms and degradation.— The combined TEM/SAXS/XRD characterization of these three materials allows us to propose the nature of the particle growth processes that result in loss of active ECSA for the various implanted/non-implanted materials. The emergence of the crystalline phase on the un-doped catalyst materials supports the dissolution/re-deposition particle growth process. In comparison, the SAXS/XRD analysis for N-modified material does not show the emergence of a new particle size regime or crystalline phase. This observation suggests that agglomeration as the possible particle growth mechanism for the N-modified catalyst material. There is strong evidence that suggests that the incorporation of N-species on the carbon support surface results in improved catalyst-support interactions. These interactions play a key role in stabilization of the nano-particle catalyst phase, and may also have positive impact on dissolution energies for the metal-based nano-particle catalyst phases. The CO stripping curves in Figure 4 indicate that a majority of the surface area losses are due to the loss of Ru phases for all materials tested. This conclusion is based on the shift in the CO stripping "kick-off" and peak potentials to more positive values after the cycling protocols. It is interesting to note that the CO

stripping curves after potential cycling for the N-modified material in Figure 4c maintain CO stripping current at negative potentials, similar to the non-cycled material. Unfortunately, it is difficult to discriminate between the effects of select N surface species. DFT analysis suggests that the specific roles of pyridinic, pyrrollic, cyano, and graphic N are complex in nature and that the presence of two or more N-species may be needed to stabilize bi-metallic catalyst systems such as Pt-Ru.[27]

Conclusions

Stabilization of fuel cell catalyst particles to mitigate catalyst surface area loss during fuel cell operation is a materials engineering challenge that must be addressed to enable widespread commercialization of advanced fuel cell technologies. We have demonstrated that the manipulation of catalyst-support interactions via N-modification of support chemistry can result in improved retention of Pt-Ru particle surface area after electrochemical cycling. Based on a combined electrochemical, structural, and morphological analysis of doped vs. undoped support materials, our observations suggest that N-modified support materials mitigate catalyst surface area loss from catalyst phase dissolution and re-deposition processes in particular.

This work focused on the stabilization of catalyst phases and materials for utilization in DMFC anodes; however the concept/process of chemically modifying fuel cell catalyst supports to fabricate highly functionalized materials for energy conversion and storage technology platforms can be extended to other systems as well. Implementation of the fuel cell catalyst fabrication techniques and routes described in this work can be directly applied to material synthesis approaches for Pt-based cathode catalyst materials. It is possible that optimal N-surface functionality will vary depending on metal catalyst composition. If so, much fundamental work must be pursued to gain a better understanding of the electronic modifications that occur as a result of catalyst-support interactions.

Acknowledgments

This work was supported by the U.S. Department of Energy under Contract No. DE-AC36-08-GO28308 with the National Renewable Energy Laboratory. The SAXS and XRD work on this project by the Colorado School of Mines was supported by the Army Research office (under Grant No. W911NF-09-1-0528). Portions of this research were carried out at the Stanford Synchrotron Radiation Lightsource (SSRL), a Directorate of SLAC National Accelerator Laboratory and an Office of Science User Facility operated for the U.S. Department of Energy Office of Science by Stanford University. We acknowledge Michael Toney, Tom Hostetler, Doug Van Campen, and John Pople for useful support regarding synchrotron experiments.

References

1. Y. Zhou, R. Pasquarelli, T. Holme, J. Berry, D. Ginley, and R. O'Hayre, *Journal of Materials Chemistry*, **19**, 7830 (2009).
2. Y. Zhou, K. Neyerlin, T. S. Olson, S. Pylypenko, J. Bult, H. N. Dinh, T. Gennett, Z. Shao, and R. O'Hayre, *Energy & Environmental Science*, **3**, 1437 (2010).
3. Y. Zhou, T. Holme, J. Berry, T. R. Ohno, D. Ginley, and R. O'Hayre, *Journal of Physical Chemistry C*, **114**, 506 (2009).
4. S. Pylypenko, A. Queen, T. S. Olson, A. Dameron, K. O'Neill, K. C. Neyerlin, B. Pivovar, H. N. Dinh, D. S. Ginley, T. Gennett, and R. O'Hayre, *Journal of Physical Chemistry C*, **115**, 13676 (2011).
5. H. A. Gasteiger, N. Markovic, P. N. Ross, and E. J. Cairns, *Electrochimica Acta*, **39**, 1825 (1994).
6. H. A. Gasteiger, N. Markovic, P. N. Ross, and E. J. Cairns, *Journal of Physical Chemistry*, **98**, 617 (1994).
7. T. T. H. Cheng, N. Jia, and P. He, *Journal of the Electrochemical Society*, **157**, B714 (2010).
8. T. T. H. Cheng, N. Jia, V. Colbow, S. Wessel, and M. Dutta, *Journal of Power Sources*, **195**, 4622 (2010).
9. P. Piela, C. Eickes, E. Brosha, F. Garzon, and P. Zelenay, *Journal of the Electrochemical Society*, **151**, A2053 (2004).
10. S. Pylypenko, A. Queen, T. S. Olson, A. Dameron, K. O'Neill, K. C. Neyerlin, B. Pivovar, H. N. Dinh, D. S. Ginley, T. Gennett, and R. O'Hayre, *Journal of Physical Chemistry C*, **115**, 13667 (2011).
11. G. S. Szymanski, T. Grzybek, and H. Papp, *Catalysis Today*, **90**, 51 (2004).
12. B. Stohr, H. P. Boehm, and R. Schlogl, *Carbon*, **29**, 707 (1991).
13. V. V. Strelko, V. S. Kuts, and P. A. Thrower, *Carbon*, **38**, 1499 (2000).
14. C.-H. Wang, H.-C. Shih, Y.-T. Tsai, H.-Y. Du, L.-C. Chen, and K.-H. Chen, *Electrochimica Acta*, **52**, 1612 (2006).
15. G. Wu, D. Li, C. Dai, D. Wang, and N. Li, *Langmuir*, **24**, 3566 (2008).
16. B. Yue, Y. Ma, H. Tao, L. Yu, G. Jian, X. Wang, X. Wang, Y. Lu, and Z. Hu, *Journal of Materials Chemistry*, **18**, 1747 (2008).
17. T. Maiyalagan, *Applied Catalysis B-Environmental*, **80**, 286 (2008).
18. H. Y. Du, C. H. Wang, H. C. Hsu, S. T. Chang, U. S. Chen, S. C. Yen, L. C. Chen, H. C. Shih, and K. H. Chen, *Diamond and Related Materials*, **17**, 535 (2008).
19. R. Chetty, S. Kundu, W. Xia, M. Bron, W. Schuhmann, V. Chirila, W. Brandl, T. Reinecke, and M. Muhler, *Electrochimica Acta*, **54**, 4208 (2009).
20. Z. Lei, L. An, L. Dang, M. Zhao, J. Shi, S. Bai, and Y. Cao, *Microporous and Mesoporous Materials*, **119**, 30 (2009).
21. Z. Lei, M. Zhao, L. Dang, L. An, M. Lu, A.-Y. Lo, N. Yu, and S.-B. Liu, *Journal of Materials Chemistry*, **19**, 5985 (2009).
22. S. Suthirakun, T. Sarakonsri, S. Aukkaravittayapun, and T. Vilaithong, *Journal of Ceramic Processing Research*, **10**, 502 (2009).
23. G. Wu, R. Swaidan, D. Li, and N. Li, *Electrochimica Acta*, **53**, 7622 (2008).
24. A. A. Dameron, T. S. Olson, S. T. Christensen, J. E. Leisch, K. E. Hurst, S. Pylypenko, J. B. Bult, D. S. Ginley, R. P. O'Hayre, H. N. Dinh, and T. Gennett, *Acs Catalysis*, **1**, 1307 (2011).
25. S. Pylypenko, B. B. Blizanac, T. S. Olson, D. Konopka, and P. Atanassov, *Acs Applied Materials & Interfaces*, **1**, 604 (2009).
26. N. Wongyao, A. Therdthianwong, and S. Therdthianwong, *Fuel*, **89**, 971 (2010).
27. T. Holme, Y. Zhou, R. Pasquarelli, and R. O'Hayre, *Physical Chemistry Chemical Physics*, **12**, 9461 (2010).